

Blast resistance of a ceramic-metal armour subjected to air explosion: A parametric study

Mohammad Javad Rezaei^{1a}, Mahdi Gerdooei^{*1} and Hasan Ghaforian Nosrati^{2b}

¹Faculty of Mechanical and Mechatronics Engineering, Shahrood University of Technology, Shahrood, Iran

²Department of Mechanical Engineering, Esfarayen University of Technology, Esfarayen, North Khorasan, Iran

(Received May 12, 2019, Revised December 9, 2019, Accepted December 28, 2019)

Abstract. Nowadays, composite plates are widely used as high-strength structures to fabricate a dynamic loading-resistant armours. In this study, the shock load is applied by an explosion of spherical TNT charge at a specified distance from the circular composite plate. The composite plate contains a two-layer ceramic-metal armour and a poly-methyl methacrylate (PMMA) target layer. The dynamic behavior of the composite armour has been investigated by measuring the transferred effective stress and maximum deflection into the target layer. For this purpose, the simulation of the blast loading upon the composite structure was performed by using the load-blast enhanced (LBE) procedure in Ls-Dyna software. The effect of main process parameters such as the thickness of layers, and scaled distance has been examined on the specific stiffness of the structure using response surface method. After validating the results by comparing with the experimental results, the optimal values for these parameters along with the regression equations for transferred effective stress and displacement to the target have been obtained. Finally, the optimal values of input parameters have been specified to achieve minimum transferred stress and displacement, simultaneously with reducing the weight of the structure.

Keywords: shock wave; composite armour; ceramic-metal; optimization; response surface method

1. Introduction

In the blasting process, high-speed deformation causes a large strain rate, very high temperatures and pressure (Keshavarz, 2007). This condition transforms the explosion phenomenon into a complex and very nonlinear process for simulation. The Ls-Dyna hydrocode has a very high potential for solving nonlinear dynamic problems. This software has the ability to analyze the shock wave propagation, metals forming with large deformation, collisions, and projectiles penetration (Manual, 2012). One of the applicable approaches which can be used to determine the behavior of the structures subjected to blast loads is to simplify the load and geometry of the model instead of a real complex structure.

Rolled Homogeneous Armour (RHA) steel, is a kind of single-layer armour steel, with improved mechanical properties by hot rolling process. These types of steel are used in the body of tanks, vehicles and military equipment. Nevertheless, due to the necessity of protecting the armour structure against both the ballistic impact and explosive shock wave, it led to the employing of multi-layered structures instead of single-layer ones. Composite armours which is known as multi-layer armoured systems, consist of a hard ceramic layer and a back plate of metal or fiber-reinforced composite. The main application of the ceramic

layer is to reduce the pressure applied to the back plate, by deflection and projectile erosion. Also, metallic plates are used as the back plate to improve the tensile strength of the structure and to reduce deformation (Gooch *et al.* 1999).

Numerical and experimental investigation of the dynamic response of constrained single-layer circular plates under air blast loading at the close-range spherical charge was performed by Neuberger *et al.* (Neuberger *et al.* 2007). They used well-known Hopkinson scaling law (A. J. Wang & Hopkins, 1954) with considering the overall effect to the strain rate sensitively and variability of material properties with plate thickness on the response of the scaled model. Zamani *et al.* (2015) investigated the maximum deflection of circular aluminum plates subjected to the free air explosion, numerically and experimentally. The purpose of their implementation of experiments was to investigate the effect of waves on the deformation behavior and to extract semi-empirical model predicting the maximum deflection of the center of the circular plate subjected to the uniform and nonuniform normal shock wave. In another research, the effect of impedance and various thickness of layers on the deflection of the target plate in layered armour systems under explosive loading has been done numerically by Zamani *et al.* (2015). Their research aimed to study the behavior of multi-layer structures at high strain rates and their effect on shock wave damping and deformation of the target plate. Impact of composite materials on buried structures performance against blast wave was an investigation performed by Mazek and Wahab (2015). Lotfi and Zahrai (2018) studied the performance of blast behavior of steel infill panels with various thickness and stiffener arrangement. Fallah *et al.* (2017) investigated the

*Corresponding author, Ph.D., Assistant Professor
E-mail: Gerdooei@shahroodut.ac.ir

^a M.Sc. Student

^b Instructor, Ph.D. Student

deflection of two mild and armoured steels under localized air blast loading numerically and compared the results with the experiments. In a numerical study, Isa *et al.* (2018) compared the shock wave explosive response of a single-layer structure (RHA steel) with coupled RHA and sandwich composite panel. They found out that the coupled structure had a high potential of shock attenuation against the blast loading. Numerical simulation of the blast loading on two composite structures of flat plate and hemisphere shell was performed by Haghi *et al.* (2017). They found that hemisphere composite shell under the same load has a better resistance against blast loads in comparison to the flat plates.

Up to now, few studies have been presented about the optimization of ceramic-metal composite structures subjected to the blast loading. Therefore, in the present paper, in order to obtain an optimized armour, the effect of process variables such as composite thickness and scaled distance (the ratio of the stand-off distance to the cube root of the charge weight) has been investigated on the transmitted effective stress and displacement of the target layer. For this purpose, the numerical simulation, as well as the statistical optimization has been employed.

2. Finite element method

The finite element model (FEM) has been generated by pre-processing software of Ls-PrePost-6.1, and the nonlinear dynamics solver of Ls-Dyna was used to execute the code. In the simulation of air blasting problems, the shock load can be modeled by using two different techniques of Load-Blast (LB) and Load-Blast-Enhanced (LBE). In these two methods, a mathematical function is used to apply compressive pressure load created from the air explosion. In the LB method, the function provided by Randers-Pehrson and Bannister (1997) is employed, which is known as Brode function. It is suitable for engineering studies, the response of vehicles and structures against the landmines explosion. The LBE method uses a function to apply compressive loads due to an explosion in the air, the same as the previous method. However, this method uses an advanced function that makes it possible to consider reflected pressure waves, multiple explosive sources and moving explosive warheads. This function is known as the ConWep equation. The ConWep equation is developed by Kingery and Bulmash (1984).

In the present study, the LBE method and the ConWep equation were used to simulate the blast shock wave and to calculate the air pressure from the explosion of a spherical charge. The typical pressure-time history, $p(t)$, in air explosion can be expressed as follows (Kinney and Graham, 1985):

$$p(t) = P_0 + P_m \left[1 - \left(\frac{t}{t_d} \right) e^{-\alpha t/t_d} \right] \quad (1)$$

where P_0 , t , and t_d are the reference ambient pressure, the instantaneous time, and the positive phase duration, respectively. Also, α is called the waveform number and depends on the peak incident pressure, P_m . The waveform

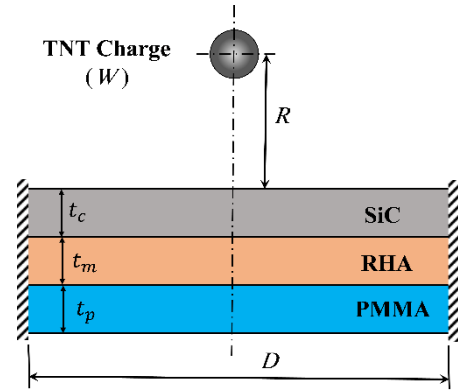


Fig. 1 Setup of structure in free air explosion

number is considered as an adjustable parameter which is selected so that the overpressure–time relationships provide suitable values of the blast impulse.

In Fig. 1 the spherical TNT charge and the composite structure are schematically displayed. D , t_c , t_m , t_p , W , and R are the diameter of plate, ceramic layer thickness, steel layer thickness, the target layer thickness, charge weight, and the distance between the charge center to the plate face, respectively. The composite structure consists of a two-layer ceramic-metal armour and a poly-methyl methacrylate (PMMA) target layer. The face plate is a silicon carbide (SiC) and the back plate is RHA steel.

To describe the constitutive model of RHA steel and the PMMA target layer, the Johnson-Cook (J-C) constitutive model has been used. This model was presented by Johnson and Cook in 1983, and has been widely used in FEM for plastic deformation at high strain rates. The J-C model is stated as follows (Zhang *et al.* 2015):

$$\sigma = [A + B\varepsilon_p^n] \left[1 + c \ln \frac{\dot{\varepsilon}_p}{\dot{\varepsilon}_0} \right] \left[1 - \left(\frac{T - T_{room}}{T_{melt} - T_{room}} \right)^m \right] \quad (2)$$

where A , B , c , n , and m are the five material constants, σ is flow stress, ε_p is the effective plastic strain, $\dot{\varepsilon}_p/\dot{\varepsilon}_0$ is the dimensionless plastic strain rate for $\dot{\varepsilon}_0 = 1 \text{ s}^{-1}$, T , T_{room} and T_{melt} are the material temperature, room temperature and melting temperature, respectively.

For modelling the material behavior of SiC ceramic, the Johnson-Holmquist (J-H) model has been used. This constitutive model is suitable to predict the behavior of brittle materials subjected to very intense loading. The J-H model can be described as follows (Holmquist and Johnson, 2002):

$$\sigma^* = \sigma_i^* - D(\sigma_i^* - \sigma_f^*) \quad (3)$$

where σ_i^* , σ_f^* , and D are effective normal stress, fracture stress, and damage parameter, respectively. Effective normal stress and fracture stress can be obtained by Eqs. (4)-(5), respectively (Holmquist and Johnson, 2002):

$$\sigma_i^* = A(P^* + T^*)^N (1 + C_0 \ln \dot{\varepsilon}^*) \quad (4)$$

$$\sigma_f^* = B(P^*)^M (1 + C_0 \ln \dot{\varepsilon}^*) \quad (5)$$

where A , B , C_0 , M , and N are the J-H material coefficients,

P^* is the normal pressure and T^* is the hydrostatic stress. $\dot{\varepsilon}^*$ is the dimensionless strain rate. The damage parameter for the J-H and J-C model can be similarly obtained as follows (Johnson and Cook 1985):

$$D = \sum \frac{\Delta \varepsilon_p}{\varepsilon_p^f} \quad (6)$$

where $\Delta \varepsilon_p$ is the increment of equivalent plastic strain during a cycle of integration changing from the start point until the failure strain, and ε_p^f is the equivalent plastic strain at failure under a constant pressure. The failure strain, ε_p^f , for the J-H is calculated as follows (Holmquist and Johnson, 2002):

$$\varepsilon_p^f = D_1 (\bar{T} + P^*)^{D_2} \quad (7)$$

where D_1 and D_2 are material coefficients, \bar{T} is the maximum normalized tensile strength, and the normalized pressure is defined as $P^* = P/P_{HEL}$, where P_{HEL} is the pressure component at the Hugoniot elastic limit.

Failure strain, ε_p^f , for the J-C model is given as (Johnson and Cook, 1985):

$$\varepsilon_p^f = [D_1 + D_2 \exp(D_3 \sigma^*)] \left[1 + D_4 \ln \left(\frac{\dot{\varepsilon}_p}{\dot{\varepsilon}_0} \right) \right] [1 + D_5 T^*] \quad (8)$$

where D_1 to D_5 are the material constants. The dimensionless pressure-stress ratio is defined as $\sigma^* = \sigma_m / \bar{\sigma}$, where σ_m is the average of the three normal stresses and $\bar{\sigma}$ is the von-Mises equivalent stress. The dimensionless plastic strain rate, $\dot{\varepsilon}_p / \dot{\varepsilon}_0$, and the homologous temperature, T^* , are identical to those used in the strength model of Eq. (2).

In addition to J-C constitutive model, the Gruneisen equation of state has been used for RHA steel. This equation for compressed and expanded state are expressed as Eq. (9) and Eq. (10) (Zhang *et al.* 2017):

$$p = \frac{\rho_0 c_0^2 \mu \left[1 + \left(1 - \frac{\gamma_0}{2} \right) \mu - \frac{a}{2} \mu^2 \right]}{\left[1 - (S_1 - 1) \mu - S_2 \frac{\mu^2}{\mu + 1} - S_3 \frac{\mu^3}{(\mu + 1)^2} \right]^2 + (\gamma_0 + a \mu) \bar{E}} \quad (9)$$

$$p = \rho_0 c_0^2 \mu + (\gamma_0 + a \mu) \bar{E} \quad (10)$$

where \bar{E} is the specific internal energy per unit volume, c_0 is the sound velocity, S_1 , S_2 and S_3 are fitting coefficients, γ_0 is Gruneisen coefficient, and a is volume correction coefficient. In the compression phase μ will be equal to $\eta - 1$, where η is the ratio of density before and after the explosion.

Table 1 shows the constants of the J-C and J-H constitutive models for RHA steel and SiC ceramic, as well as the constants of the Gruneisen equation for steel. The physical and mechanical properties of RHA steel (Neuberger *et al.* 2007), SiC ceramic (Shackelford *et al.* 2016) and PMMA plate (Dorogoy, Rittel and Brill, 2010) are presented in Table 2.

Table 1 Constants of the J-C model (Robbins *et al.* 2004) and the Gruneisen state (Wiśniewski and Tomaszewski, 2009) for RHA and constants of the J-H model (Wang and Yang, 2008) for SiC

Constants	RHA (J-C and Gruneisen)	SiC (J-H)
A (MPa)	792	0.96
B (MPa)	509	0.35
N	-	0.65
n	0.26	-
c	0.014	-
C_0	-	0
M	0	1
m	1.03	-
$\dot{\varepsilon}_0$ (S ⁻¹)	1	-
T_{melt} (K)	1793	-
T_{room} (K)	298	-
SF_{MAX}	-	0.8
HEL (GPa)	-	14.5
P_{HEL} (GPa)	-	5.9
\bar{T}	-	0.37
D_1	0.05	0.48
D_2	3.44	0.48
D_3	-2.11	-
D_4	0.002	-
D_5	0.61	-
K_1 (GPa)	-	204
c_0 (m/s)	4610	8480
S_1	1.73	-
γ_0	1.67	-

Table 2 Physical and mechanical properties of different plates

	RHA (Neuberger, 2007)	SiC (Shackelford, 2016)	PMMA (Dorogoy, 2010)
Density (kg/m ³)	7838	3163	1190
Elastic modulus (GPa)	210	429	5.76
Shear modulus (GPa)	-	370	-
Poisson's ratio	0.28	0.14	0.42
Yield strength (MPa)	950	-	64.8
Tensile strength (MPa)	-	137	-

3. Response surface method

Design of experiments (DOE) involves a series of experiments that deliberately create changes in the input variables of the process, through which the amount of variation in the output response is observed and identified. The response surface method (RSM) is a set of

mathematical and statistical techniques for modelling to analysing problems that the response is influenced by several variables. The aim of this method is model and optimize the response (Fedosov, 1999). In many problems of the RSM, the relationship between the response and the independent variables is unknown. Therefore, the first step in RSM is to find the appropriate estimate for the true functional relationship between the response and the set of independent variables. Usually, a low-order polynomial is used in some regions of independent variables. If the response is well modelled by a linear function according to independent variables, then the approximating function for the first-order model is as follows (Moradi and MohazabPak, 2018):

$$y = \beta_0 + \beta_1 x_1 + \beta_2 x_2 + \dots + \beta_k x_k + \varepsilon \quad (11)$$

where y is response function, x_1 up to x_k are independent variables, k is the number of independent variables, β_0 up to β_k are unknown fixed coefficients which obtained from the analysis, and ε is the statistical error. If there is a nonlinearity in the system, then it should be used higher order polynomials, such as the second-order model (Azadi *et al.* 2009):

$$y = \beta_0 + \sum_{i=1}^k \beta_i x_i + \sum_{i=1}^k \beta_{ii} x_i^2 + \sum_i \sum_j \beta_{ij} x_i x_j \quad (12)$$

Almost in all RSM problems, one or both of the expressed models are used. Of course, it is unlikely that a polynomial model is an acceptable approximation for the true functional relationship in all independent variables, but for a relatively small region, it usually works well (Montgomery, 2012). The RSM method is divided into various designs such as Central Composite and Box-Behnken. One of the important and most practical ones is the Central Composite Design (CCD) method, which by considering the number of independent variables and their range, designs the test matrix. In this method, different levels for each variable based on different design parameter (α) will be created. By considering the Face-Centered Cube (FCC) and $\alpha = 1$, the number of levels is 3, otherwise, the number of levels will be 5. The design matrix for the present study will have 3 different levels for each independent variables according to Table 3. The range of steel layer thickness, ceramic layer thickness, and the scaled distance are 10-20 mm, 5-15 mm, and 1.4-1.6 kg/m^{1/3}, respectively. The scaled distance variable is the ratio of the stand-off distance to the cube root of the charge weight obtained by Eq. (13) (Rajendran and Lee, 2009):

$$Z = \frac{R}{\sqrt[3]{W}} \quad (13)$$

where R and W are the stand-off distance and the charge weight, respectively.

With assuming constant TNT charge weight, the effect of these three parameters will be investigated on response variables including von-Mises effective stress (σ) and displacement (δ) created in the PMMA target layer with a constant thickness $t_p = 20$ mm. The designed experiments along with the related responses are shown in Table 4.

Table 3 Independent process parameters with design levels

Parameters	Levels		
	Low(-1)	Central(0)	High(+1)
Steel layer thickness (t_m)	10	15	20
Ceramic layer thickness (t_c)	5	10	15
Scaled distance (Z)	1.4	1.5	1.6

Table 4 Designed experiments by using the RSM method along with the response of each test

Test No.	Variables			Response	
	t_m (mm)	t_c (mm)	Z (kg/m ^{1/3})	$\bar{\sigma}$ (MPa)	δ (mm)
1	15	10	1.5	5.58	5.6
2	10	15	1.6	3.18	3.1
3	15	5	1.5	9.60	11.1
4	10	10	1.5	6.13	6.3
5	15	10	1.5	5.58	5.6
6	10	5	1.6	9.90	11.6
7	15	10	1.4	6.10	6
8	15	10	1.5	5.58	5.6
9	20	10	1.5	5.15	5.1
10	15	10	1.5	5.58	5.6
11	20	15	1.4	3.15	3
12	15	15	1.5	3.14	3.1
13	15	10	1.5	5.58	5.6
14	20	5	1.4	9.46	10.8
15	20	5	1.6	8.76	9.6
16	10	15	1.4	3.77	3.6
17	15	10	1.6	5.12	5.2
18	10	5	1.4	10.70	13
19	15	10	1.5	5.58	5.6
20	20	15	1.6	2.67	2.5

Finally, using the above mentioned results, the mathematical model for these experiments will be created by means of second order linear regression equation passing through the data points of the table or located in the nearest position of them. The Minitab-18 software was used to analyse and interpret the results, as well as obtain the coefficient of governing equations on the experiments. Also, the optimal values for achieving the minimum transferred effective stress and displacement of the target layer are presented.

4. Results and discussion

4.1 Verification of results

The simulation of a single-layer RHA plate with a spherical charge is verified with the Neuberger experimental results (Neuberger *et al.* 2007). The geometrical dimensions as well as related charge weight (W) are presented in Table 5. Fig. 2 shows the comparison

Table 5 Amount of variables for verify simulation

t (m)	D (m)	W (kg)	R (m)
0.02	1	8.75	0.13

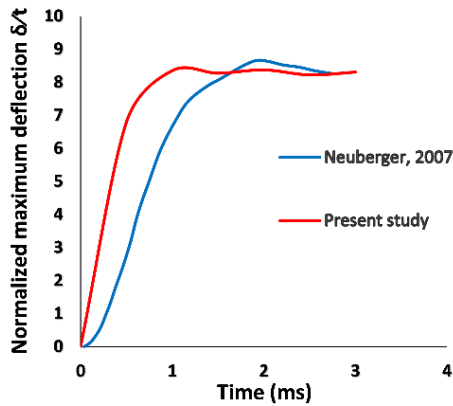


Fig. 2 Comparison between present study and experimental result for normalized deflection of a RHA plate subjected to air blasting shock

of the normalized displacement between the current study and the experimental results of Neuberger. As shown in Fig. 2 the maximum normalized displacements are equal to 8.25 and 8.23 for the experimental and numerical results, respectively. The percent of error is 0.2% indicating the reasonable accuracy of the simulation.

4.2 Analysis of variance

A reasonable judgment from the statistical results requires the confirmation of the main effects of the factors by analysis of the variance (ANOVA). These data are statistically valid when they have a normal distribution, and the variances are equal. These assumptions were verified by investigation plots of normal probability versus residual and residual versus fitted value for the maximum displacement of the PMMA target. The absence of outlying points in Fig. 3(a) represents the normality assumption. Also, the data in Fig. 3(b) are structureless representing the independence assumption. By proving the validity of these assumptions, it can be trusted to the results of ANOVA tables. It should be noted that in the ANOVA, according to the selected confidence level of 95%, a prerequisite for a model to be significant is that the amount of its p-value is less than 0.05. Based on this, one can ignore the effects of the factors with P-value greater than 0.05.

The effect of the blasting phenomenon as a complex and non-linear process depends on the different factors such as stand-off distance, structure material, number and thickness of layers. In a constant explosive charge mass, the severity of the damage increases with decreasing the stand-off distance and structure layers thickness. For accurate analysis of the effective parameters, the main effects and productive interactions between the factors are presented.

In the following, the ANOVA table for effective stress of the target layer is presented in Table 6. It can be seen that among the input variables, the ceramic layer thickness (t_c)

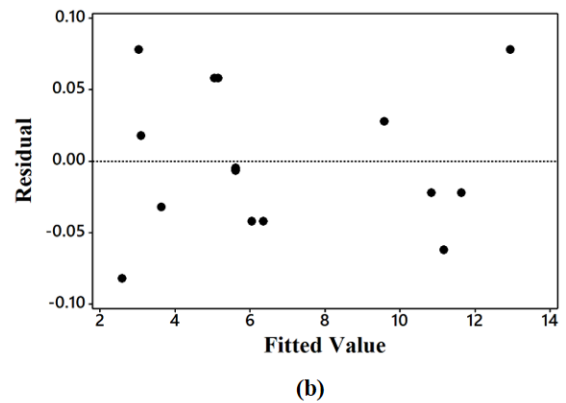
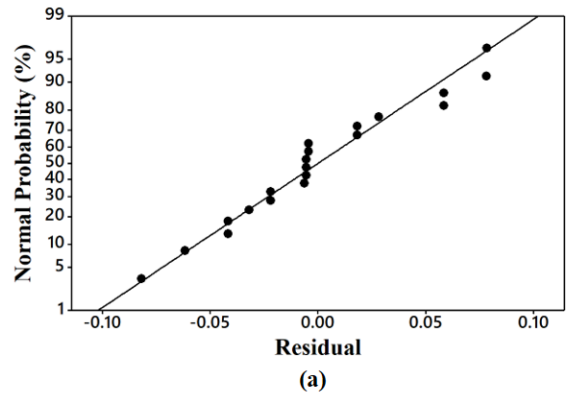


Fig. 3 a) Normal probability plot of residuals. b) residual versus fitted value plot for maximum displacement of the PMMA target

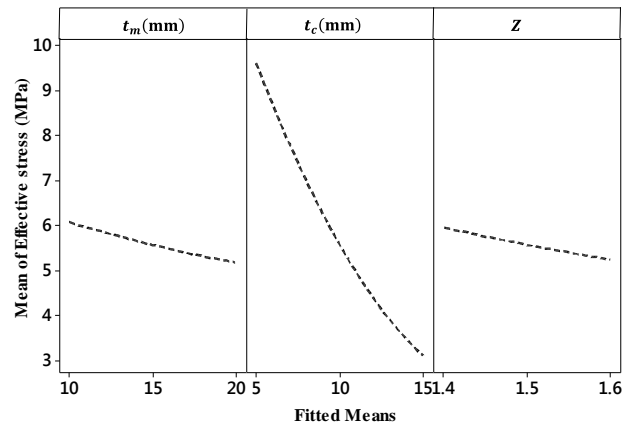


Fig. 4 Main effect of parameters on the generated effective stress in the target layer

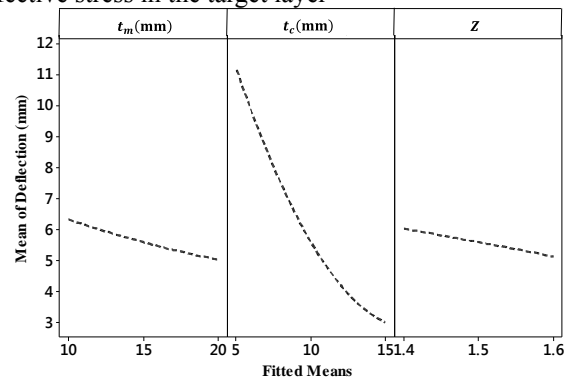


Fig. 5 Main effect of parameters on the maximum displacement of the target layer

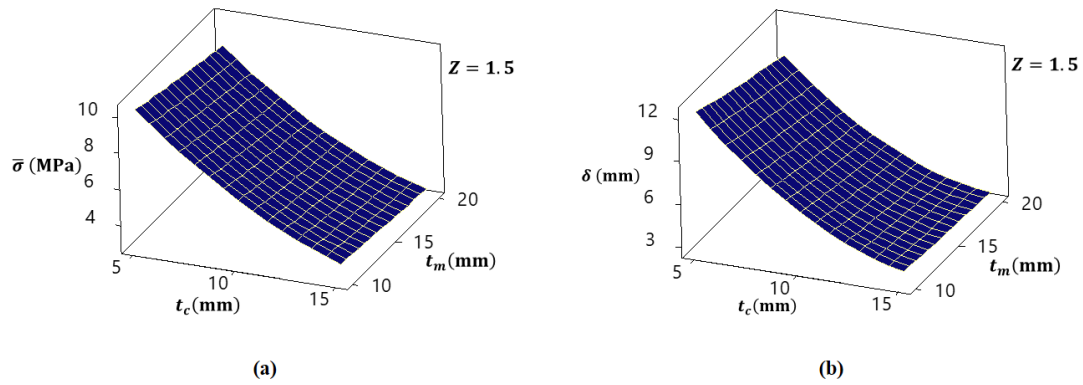


Fig. 6 Response surface graph based on the RHA and SiC thicknesses for a) the effective stress and b) the maximum displacement of target

Table 6 ANOVA table for effective stress of the target layer

Source	DF	Seq. SS	Contribution	P-Value
Model	9	112.692	99.95%	0.000
Linear	3	108.966	96.65%	0.000
t_m	1	2.016	1.79%	0.000
t_c	1	105.690	93.74%	0.000
Z	1	1.260	1.12%	0.000
Square	3	3.502	3.11%	0.000
t_m^2	1	1.474	1.31%	0.223
t_c^2	1	2.026	1.80%	0.000
Z^2	1	0.002	0.00%	0.561
2-Way Interaction	3	0.224	0.20%	0.001
$t_m \times t_c$	1	0.195	0.17%	0.000
$t_m \times Z$	1	0.006	0.00%	0.323
$t_c \times Z$	1	0.023	0.02%	0.059
Error	10	0.051	0.05%	
Lack-of-Fit	5	0.051	0.05%	0.000
Pure Error	5	0.00	0.00%	
Total	19	112.743	100.00%	

has the most effect on the effective stress of the target layer with 93.74% contribution. All the second-order parameters (t_m^2, z^2) other than (t_c^2), do not have a significant effect on the process, as regards that their P-value is not less than 0.05. Moreover, while the effects of interactions $t_m \times Z$ and $t_c \times Z$ are not significant, a little interaction can be observed between t_m and t_c .

Table 7 represents the ANOVA table of maximum displacement of the target layer. The results show that the most significant effect was related to the ceramic layer thickness with 89.47% contribution. All parameters other than the second-order parameter Z^2 and the interaction effect between $t_m \times Z$ have a little bit effect on the amount of target layer displacement.

The Eqs. (14)-(15) describe the regression equations of response functions based on the analysis of variance. Amounts of R-Sq(adj) and R-Sq for effective stress value are 99.91% and 99.95%, respectively; and for the displacement of the target layer are 99.96% and 99.98%,

Table 7 ANOVA table for the displacement of the target layer

Source	DF	Seq. SS	Contribution	P-Value
Model	9	185.107	99.98%	0.000
Linear	3	171.899	92.85%	0.000
t_m	1	4.225	2.28%	0.000
t_c	1	165.649	89.47%	0.000
Z	1	2.025	1.09%	0.000
Square	3	11.725	6.33%	0.000
t_m^2	1	4.704	2.54%	0.040
t_c^2	1	7.021	3.79%	0.000
Z^2	1	0.001	0.00%	0.715
2-Way Interaction	3	1.484	0.80%	0.000
$t_m \times t_c$	1	1.201	0.65%	0.000
$t_m \times Z$	1	0.001	0.00%	0.572
$t_c \times Z$	1	0.281	0.15%	0.000
Error	10	0.037	0.02%	
Lack-of-Fit	5	0.037	0.02%	0.000
Pure Error	5	0.000	0.00%	
Total	19	185.144	100.00%	

respectively. Therefore, modelling by using the response surface method indicates desirable accuracy.

$$\begin{aligned} \bar{\sigma} = & 31.96 - 0.2981 t_m - 1.5339 t_c - 13.2 Z \\ & + 0.00224 t_m^2 + 0.03144 t_c^2 \\ & + 2.59 Z^2 + 0.00625 (t_m \times t_c) \\ & + 0.0525 (t_m \times Z) \\ & + 0.1075 (t_c \times Z) \end{aligned} \quad (14)$$

$$\begin{aligned} \delta = & 34.6 - 0.4261 t_m - 2.7981 t_c - 4.5 Z \\ & + 0.00345 t_m^2 + 0.05945 t_c^2 \\ & - 1.37 Z^2 + 0.0155 (t_m \times t_c) \\ & + 0.025 (t_m \times Z) + 0.375 (t_c \times Z) \end{aligned} \quad (15)$$

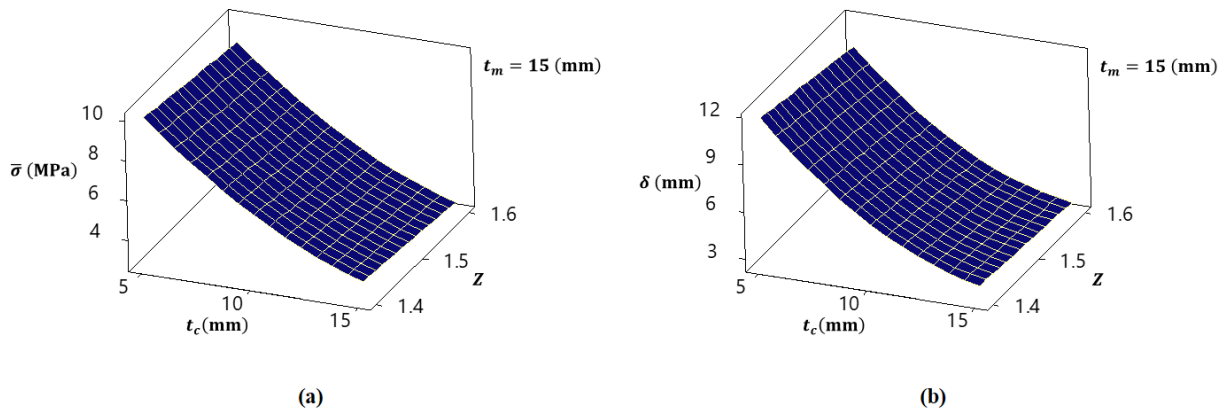


Fig. 7 Response surface graph based on the SiC thickness and the scaled distance for a) the effective stress and b) the maximum displacement of the target layer

4.3 Main effects

In the DOE method evaluating the effect of each factor can be represented and interpreted by the main effect plot of each response. In Fig. 4 the main effect plot of independent variables, i.e. layer thicknesses and scaled distance (Z) are shown on the magnitude of the transmitted effective stress in the target layer. It can be seen that by increasing the thickness of the both layers, the transmitted effective stress decreases, due to the strengthening of the armour composite, while the effect of face ceramic plate is more significant than that of metallic back plate. Indeed, by increasing the ceramic layer thickness from 5 mm to 15 mm, the transmitted effective stress decreases almost from 9.5 MPa to 3 MPa. The comparison between the contribution percentage of t_m and t_c in Table 6 confirms this issue. The similar discussion can be drawn for the maximum displacement of the target layer as shown the main effect of parameters in Fig. 5.

The 3D surface graph of $\bar{\sigma}$ and δ versus ceramic thickness and metal thickness are presented in Fig. 6. In these plots, the Z parameter is supposed to have a constant value of 1.5. According to Fig. 6-a, the maximum effective stress in PMMA target will be created when the RHA and SiC layers have the lowest thicknesses due to the least strength of plate in this condition.

Similarly, the 3D plots of responses versus the SiC layer thickness and the scaled distance Z for fixed RHA layer thickness of 15 mm have been shown in Fig. 7. It can be clearly observed that independent to the Z parameter, increasing the ceramic thickness leads to strengthen the armour structure and to decrease both the target displacement and effective stress. Moreover the effect of scaled distance Z is negligible in comparison to the ceramic layer thickness.

4.4 Optimal condition

The goal of the optimization in the dynamic response of the composite structure is to minimize the transmitted effective stress and displacement, in addition to maximizing the amount of the specific stiffness (the ratio of the stiffness

to the weight of the armour structure). However, in practice, it is not possible to gain the optimal amounts for all of the responses due to the reverse effects of process parameters on each response. In other words, the improvement of one response has an inevitable adverse effect on another one. Therefore, the next step is to select the optimal levels to obtain the maximum desirability; i.e. all responses achieve an acceptable level of satisfaction. Response optimization tries to identify the best combination of the input variables that jointly optimize a single response or a set of responses. Individual desirability (d) evaluates how the settings optimize a single response, while composite desirability (D) evaluates how the settings optimize a set of responses. Desirability has a range of zero to one and one represents the ideal case. Eq. (16) shows their relation:

$$D = (d_1 d_2 \cdots d_m)^{\frac{1}{m}} \quad (16)$$

Optimality evaluation is performed using “response optimizer” in Minitab software. It should be mentioned that for each case, the specific stiffness (S^*) was defined according to Eq. (17) and utilized as a determinant parameter. In Eq. (18) W_s is the weight of the composite structure and S is the stiffness of the structure calculated by Eq. (18) (Wyser, Pelletier and Lange 2001):

$$S^* = \frac{S}{W_s} \quad (17)$$

$$S = \frac{EI}{b} \quad (18)$$

where E , I , and b are the elastic modulus, the moment of inertia and width of the structure, respectively. The optimal levels and corresponding predicted responses for different values of scaled distances are reported in Table 8.

In order to confirm the prediction of the optimization method, the simulation of the blast loading on the optimized structure has been performed considering both response parameters of effective stress and maximum displacement. The FEM results are presented in the fourth column of Table 8. In the last column of the table the estimated

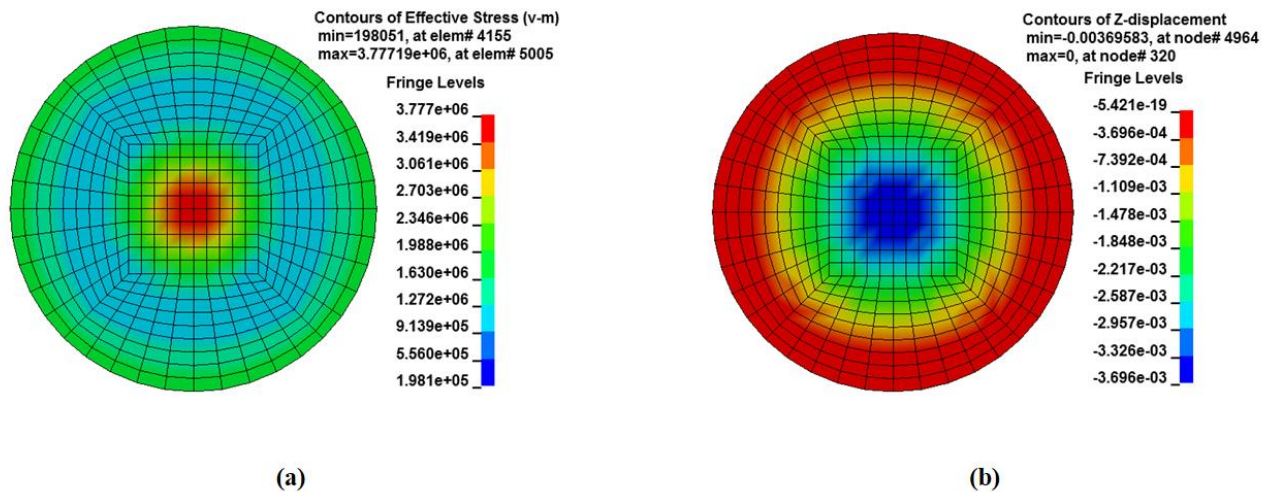


Fig. 8 Contour plot of a) effective stress (Pascal) and b) maximum normal displacement (meter), in PMMA target under optimal conditions for $Z = 1.4$

Table 8 Optimal values of design factors, as well as the related responses, comparison between the prediction of regression and FEM

Const. factor	Optimal values (mm), $W_s(N)$, $S^*(N.m/N)$	Response values $\delta(mm)$, $\sigma(MPa)$	FEM values $\delta(mm)$, $\sigma(MPa)$	Diff. (%)
$Z = 1.4$	$t_m = 10$	$\sigma = 3.81$	$\sigma = 3.77$	1
	$t_c = 15$			
	$S^* = 415.37$	$\delta = 3.63$	$\delta = 3.70$	2
	$W_s = 969.45$			
$Z = 1.6$	$t_m = 10$	$\sigma = 3.16$	$\sigma = 3.18$	0.6
	$t_c = 15$			
	$S^* = 415.37$	$\delta = 3.08$	$\delta = 3.10$	0.6
	$W_s = 969.45$			

optimum responses are compared with the FEM result. The maximum percent of variation is equal to 2% indicating the accuracy of the optimization results.

The contour plots of the effective stress and normal displacement at the PMMA plate corresponding with the optimal conditions for $Z = 1.4$ have been presented in Fig. 8-a and Fig. 8-b, respectively. It can be seen, while the maximum effective stress and displacement are generated at the center of the plate, no damage occurred all over the composite plate.

5. Conclusions

In this research, the response of a ceramic/metal composite armour subjected to the air blast shock wave has been investigated. The effect of the ceramic face thickness, the metallic back plate thickness, and the scaled charge distance on the effective transmitted stress and maximum displacement of a polymer target have been examined by finite element simulation, and response surface method. To validate the numerical solution, the results were compared

to the experiments of the other researcher, and a good agreement was achieved. Furthermore, analysis of variance along with the considering of normal distribution of data was utilized to interpret the effectiveness of each parameter. The results showed that among the input variables, the ceramic layer thickness has the most effect on the both evaluated responses mainly the effective transmitted stress and maximum displacement occurred in the target layer. Increasing the thickness of both layers will decrease the transmitted effective stress independently to Z value, due to the strengthening of the armour composite. Nevertheless, the effect of the ceramic face plate is more significant than that of the metallic back plate. Also, the effect of scaled distance especially in the examined range of 1.4 to 1.6 can be neglected in comparison to the other factors. Finally, the Minitab optimizer was utilized to predict the optimal values of each input factors. As a result, it was indicated that the minimum distributed stress and displacement along with the maximum specific stiffness will occur when the thickness of the metal and ceramic layers are 10 mm and 15 mm, respectively. Additionally, the FEM results showed that the maximum transmitted stress and displacement were generated at the center of the plate. As well, there was no failure in either SiC face plate or RHA back plate.

References

- Aslani, A. and Zamani Ashani, J. (2015), "A numerical analysis on effect of impedance and thickness of various layers on deflection of target plate in layered armor systems under explosive loading", *J. Sci. Technol. Compos.*, **1**(2), 11–20.
- Azadi, M., Azadi, S., Zahedi, F. and Moradi, M. (2009), "Multidisciplinary optimization of a car component under NVH and weight constraints using RSM", *ASME 2009 International Mechanical Engineering Congress and Exposition*, 315–319, Florida, November.
- Dorogoy, A., Rittel, D. and Brill, A. (2010), "A Study of inclined impact in polymethylmethacrylate plates", *J. Impact Eng.*, **37**(3), 285–294.
- Fedosov, S. A. (1999), "Laser beam hardening of carbon and low

- alloyed steels: discussion of increased quantity of retained austenite”, *J. Mater. Sci.*, **34**(17), 4259–4264.
- Gooch, W. A., Chen, B. H. C., Burkins, M. S., Palicka, R., Rubin, J. J. and Ravichandran, R. (1999), “Development and Ballistic Testing of a Functionally Gradient Ceramic/Metal Applique”, *Materials Science Forum*, **308–311**, 614–621. <https://doi.org/10.4028/www.scientific.net/MSF.308-311.614>
- Holmquist, T. J. and Johnson, G. R. (2002), “Response of silicon carbide to high velocity impact”, *J. Appl. Phys.*, **91**(9), 5858–5866. <https://doi.org/10.1063/1.1468903>.
- Isa, M. F. M., Risby, M. S., Norazman, M. N., Khalis, S., Hafizi, M. N. and Arif, S. (2018), “Simulation on the shock attenuation behavior of coupled RHA and sandwich composite panel under blast loading”, *J. Fundamental Appl. Sci.*, **9**(3S), 555. <https://doi.org/10.4314/jfas.v9i3s.43>
- Johnson, G. R. and Cook, W. H. (1985), “Fracture characteristics of three metals subjected to various strains, strain rates, temperatures and pressures”, *Eng. Fracture Mech.*, **21**(1), 31–48. [https://doi.org/10.1016/0013-7944\(85\)90052-9](https://doi.org/10.1016/0013-7944(85)90052-9).
- Keshavarz, M. (2007), “Detonation velocity of pure and mixed CHNO explosives at maximum nominal density”, *J. Hazardous Mater.*, **141**(3), 536–539. <https://doi.org/10.1016/j.jhazmat.2006.07.060>
- Kingery, C. N. and Bulmash, G. (1984), *Airblast Parameters from TNT Spherical Air Burst and Hemispherical Surface Burst*, US Army Armament and Development Center, Ballistic Research Laboratory.
- Kinney, G. F. and Graham, K. J. (1985), *Explosive Shocks in Air*, Springer, Germany. <https://doi.org/10.1007/978-3-642-86682-1>
- Lotfi, S. and Zahrai, S. M. (2018), “Blast behavior of steel infill panels with various thickness and stiffener arrangement”, *Struct. Eng. Mech.*, **65**(5), 587–600. <https://doi.org/10.12989/sem.2018.65.5.587>.
- Manual, K.U.S. (2012), *LS-DYNA keyword user's manual Volume I*, Livermore Software Technology Corporation (LSTC), Livermore, CA, USA.
- Mazek, S. A. and Wahab, M. (2015), “Impact of composite materials on buried structures performance against blast wave”, *Struct. Eng. Mech.*, **53**(3), 589–605. <https://doi.org/10.12989/sem.2015.53.3.589>.
- Mehreganian, N., Fallah, A. S., Boiger, G. K. and Louca, L. A. (2017), “Response of Armour Steel Square Plates To Localised Air Blast Load- a Dimensional Analysis”, *International Journal of Multiphysics*, **11**(December), 1–20. <https://doi.org/10.21152/1750-9548.11.4.387>
- Montgomery, D. C. (2012), *Design and Analysis of Experiments* (8th ed.), Wiley, Hoboken, NJ, USA.
- Moradi, M. and MohazabPak, A. R. (2018), “Statistical Modelling and Optimization of Laser Percussion Microdrilling of Inconel 718 Sheet Using Response Surface Methodology (RSM)”, *Lasers in Engineering (Old City Publishing)*, **39**(3-6), 313-331.
- Neuberger, A., Peles, S. and Rittel, D. (2007), “Scaling the response of circular plates subjected to large and close-range spherical explosions. Part I: Air-blast loading”, *J. Impact Eng.*, **34**(5), 859–873. <https://doi.org/10.1016/j.ijimpeng.2006.04.001>.
- Rajendran, R. and Lee, J. M. (2009), “Blast loaded plates”, *Marine Struct.*, **22**(2), 99–127. <https://doi.org/10.1016/j.marstruc.2008.04.001>.
- Randers-Pehrson, G. and Bannister, K.A. (1997), “Airblast Loading Model for DYNA2D and DYNA3D”, Army Research Lab., Aberdeen Proving Ground, M.D., 15, 97.
- Haghi, R., Bashir Behjat, M. and Yazdani, M. (2017), “Numerical Investigation of Composite Structures under Blast Loading”, *J. Mater. Environ. Sci.*, **8**(6), 2231–2237.
- Robbins, J. R., Ding, J. L. and Gupta, Y. M. (2004), “Load spreading and penetration resistance of layered structures—a numerical study”. *J. Impact Eng.*, **30**(6), 593–615. <https://doi.org/10.1016/j.ijimpeng.2003.08.001>.
- Shackelford, J. F., Han, Y.H., Kim, S. and Kwon, S.H. (2016), *CRC Materials Science and Engineering Handbook*, CRC Press, Florida, USA.
- Wang, A. J. and Hopkins, H. G. (1954), “On the plastic deformation of built-in circular plates under impulsive load”, *J. Mech. Phys. Solids*, **3**(1), 22–37. [https://doi.org/10.1016/0022-5096\(54\)90036-8](https://doi.org/10.1016/0022-5096(54)90036-8).
- Wang, Y.F. and Yang, Z.G. (2008), “Finite element model of erosive wear on ductile and brittle materials”, *Wear*, **265**(5–6), 871–878.
- Wiśniewski, A. and Tomaszewski, Ł. (2009), “Analysis of penetration depth with the use of AUTODYN 5 programme”, *Problemy Techniki Uzbrojenia*, **38**(110), 47-56.
- Wyser, Y., Pelletier, C. and Lange, J. (2001), Predicting and determining the bending stiffness of thin films and laminates. *Packaging Technol. Sci.*, **14**(3), 97–108. <https://doi.org/10.1002/pts.540>.
- Zamani, J. and Goudarzi, M. (2015), “Experimental and numerical investigation of the maximum deflection of circular aluminum plate subjected to free air explosion”, *Modares Mechanical Engineering*, **15**(1), <http://journals.modares.ac.ir/article-15-10331-en.html>.
- Zhang, Y., Outeiro, J.C. and Mabrouki, T. (2015), “On the Selection of Johnson-cook Constitutive Model Parameters for Ti-6Al-4V Using Three Types of Numerical Models of Orthogonal Cutting”, *Procedia CIRP*, **31**, 112–117. <https://doi.org/https://doi.org/10.1016/j.procir.2015.03.052>.
- Zhang, Z., Wang, L. and Silberschmidt, V.V. (2017), “Damage response of steel plate to underwater explosion: Effect of shaped charge liner”, *J. Impact Eng.*, **103**, 38-49. <https://doi.org/10.1016/j.ijimpeng.2017.01.008>.

PL